An Observation System Simulation Experiment for the Impact of Land Surface Heterogeneity on AMSR-E Soil Moisture Retrieval

Wade T. Crow, Matthias Drusch, and Eric F. Wood

***Abstract*—Using a high-resolution hydrologic model, a land surface microwave emission model (LSMEM), and an explicit simulation of the orbital and scanning characteristics for the advanced microwave sensing radiometer (AMSR-E), an observing system simulation experiment (OSSE) is carried out to assess the impact of land surface heterogeneity on large-scale retrieval and validation of soil moisture products over the U.S. Southern Great Plains using the 6.925 GHz channel on the AMSR-E sensor. Land surface heterogeneity impacts soil moisture products through the presence of nonlinearities in processes represented by the LSMEM, as well as the fundamental inconsistency in spatial scale between gridded soil moisture imagery derived from *in situ* point-scale sampling, numerical modeling, and microwave remote sensing sources. Results within the 575 000 km^2 Red-Arkansas River basin show that, for surfaces with vegetation water contents below 0.75 kg/m^2, these two scale effects induce root mean squared errors (RMSEs) of 1.7% volumetric $(0.017\ \mathrm{cm}^3_{\mathrm{water}}/\mathrm{cm}^3_{\mathrm{soil}})$ into daily 60 km AMSR-E soil moisture products and RMS differences of 3.0% $(0.030\ \mathrm{cm}^3_{\mathrm{water}}/\mathrm{cm}^3_{\mathrm{soil}})$ into 60 km comparisons of AMSR-E soil moisture products and *in situ* field-scale measurements of soil moisture sampled on a fixed 25-km grid.**

***Index Terms*—Antenna gain function, hydrological modeling, passive microwave remote sensing, soil moisture.**

I. Introduction

LAND surface heterogeneity and its effect on modeling and observing surface processes has concerned climate modelers, hydrologists, and remote sensing scientists for the last twenty years [1]–[3]. The retrieval of physical climate variables from passive microwave remote sensors is of particular interest because of current antenna technology, which results in low spatial resolution footprints at frequencies suitable for remote sensing of soil moisture. The special sensor microwave/imager (SSM/I) sensor, for example, has a -3 dB resolution of $69 * 43$ km^2 at 19 GHz. While such -3 dB values are often referred to as the "effective field of view resolution" for the sensor, it is important to acknowledge that half of the information integrated by the antenna will actually come from beyond the -3 dB area [4]. Relatively coarse $(> 50^2$ km$^2)$ resolutions will characterize spaceborne passive microwave radiometers through at least the next generation of sensors. The advanced microwave sensing radiometer (AMSR-E) on the EOS-AQUA spacecraft is expected to have a -3 dB resolution of $75 * 43$ km^2 at 6.925 GHz [5]. Even the introduction of new radiometer technology, such as synthetic aperture radiometry, is not expected to reduce spatial resolutions below 10^2 to 30^2 km^2 [6]. Given such coarse spatial resolutions, the presence of spatial heterogeneity in land surface conditions (soil wetness, snow cover, vegetation cover and state) introduces a range of complexities in the retrieval and validation of passive microwave-based estimates of physical parameters like soil moisture. Underlying many of these difficulties are fundamental contrasts in measurement scales between soil moisture data derived from spaceborne microwave sensors and soil moisture information derived from other sources

Following [7], support is defined to be the spatial area over which a given measurement (or prediction technique) integrates information. The spatial support of microwave satellite data is determined by its antenna gain function and the manner in which this function assigns weight to various portions of the sensor's footprint. For AMSR-E and SSM/I antenna patterns, the gain function can be approximated by an appropriately parameterized two-dimensional (2-D) Gauss function [8]. As presently envisioned [5], the AMSR-E soil moisture validation plan relies on comparisons between satellite derived soil moisture estimates and *in situ* observations, either from operational soil moisture networks or specialized soil moisture validation networks. An implicit assumption being that point-supported *in situ* soil moisture observations, or the weighted spatial average of a set of such observations, can be scaled up to the footprint-scale $(\sim 60$ km$)$. The accuracy of this assumption depends on the spatial variability [9], [10] and autocorrelation [11] of the underlying soil moisture field as well as the methodology applied to selecting sampling sites [12].

Similar contrasts exist between the spatial support of satellite-derived parameters and the coarse (typically 10 to 100 km) numerical grids that physics-resolving climate and weather prediction models operate on. Even when satellite measurements are gridded onto the same computational grid as the numerical model, the support of the "grid-averaged" values are not consistent. The numerical model assumes that subgrid variability is averaged with equal areal weighting, while the satellite product is obtained through averaging by some combination of nonlinear antenna gain functions. As a result, there is an incompatibility between the spatial support of numerical model input/output and the spatial support of gridded fields obtained from microwave remote sensing [4].

Manuscript received October 1, 2000; revised April 20, 2001. This work was supported by NASA Grants NAG8–1517 and NAG5–6494 and NOAA Grant NA96GP0413.

W. T. Crow and E.F. Wood are with the Department of Civil and Environmental Engineering, Princeton University, Princeton, NJ 08544 USA (e-mail: wadecrow@princeton.edu).

M. Drusch is with the Meteorological Institute, Bonn University, Bonn, Germany.

Publisher Item Identifier S 0196-2892(01)06678-5.

Soil moisture values derived from microwave remote sensing and assigned to various grids will not be uniquely determined by microwave emission from within that grid, nor will they be derived from an equal weighting of emission occurring from all areas of the grid.

The coarse spatial support implied by microwave gain functions has enhanced consequences when retrieved brightness temperature values are processed through nonlinear algorithms or models. Nonlinear model physics dictate that grid-scale model output will be sensitive to the presence, or absence, of subgrid-scale spatial variability in inputs. In a soil moisture/brightness temperature context, the issue is whether a footprint-scale measurement of brightness temperature is adequate to estimate footprint-scale soil moisture or whether nonlinearities in microwave emission modeling dictate that some consideration be given to subfootprint-scale heterogeneity in soil moisture [13], vegetation [14], or soil properties [15].

The most promising sensor for microwave soil moisture remote sensing in the near future will be the 6.925 GHz AMSR-E radiometer, currently planned for launch aboard the EOS-PM (AQUA) satellite in late 2001. This sensor will be capable of providing daily brightness temperature imagery for nearly all locations on the globe [5]. Understanding the effects of different measurement supports for soil moisture fields derived from microwave remote sensors, numerical models, and point-scale *in situ* measurements is critical for evaluating the quality of large-scale soil moisture products derived from microwave remote sensors. In this paper we carry out an observing system simulation experiment (OSSE) for AMSR-E to evaluate the effect of subfootprint-scale land surface heterogeneity on the retrieval and validation of soil moisture products.

II. OSSE Procedure

The complete OSSE experiment consisted of the four parts shown in Fig. 1: a simulation of surface conditions based on hydrologic modeling, forward land surface microwave emission modeling, a simulation of AMSR-E retrieval and gridding of brightness temperature products, and backward land surface microwave emission modeling of the simulated AMSR-E brightness temperature products.

Surface conditions were derived from 1-km hydrologic modeling of the entire Red-Arkansas River basin for the time period April 1, 1994 through July 31, 1994 (Fig. 2). Modeled surface temperature (T_s) and soil moisture (θ) fields were processed through a forward land surface microwave emission model (LSMEM) to produce top of the atmosphere brightness temperature imagery (T_b). Notationally, the LSMEM will be represented by f and can be summarized as

$$f(\theta, T_s, \tilde{x}) = T_b \tag{1}$$

where $(\tilde{x})$ stands for various land surface parameters used in the forward microwave emission process. Next, an explicit simulation of AMSR-E brightness temperature sampling was performed on the simulated T_b imagery. The simulation mimiced the orbital characteristics, scan patterns, gain function sampling, and gridding procedures planned for actual AMSR-E T_b products. The spatial sampling and gridding characteristics for the

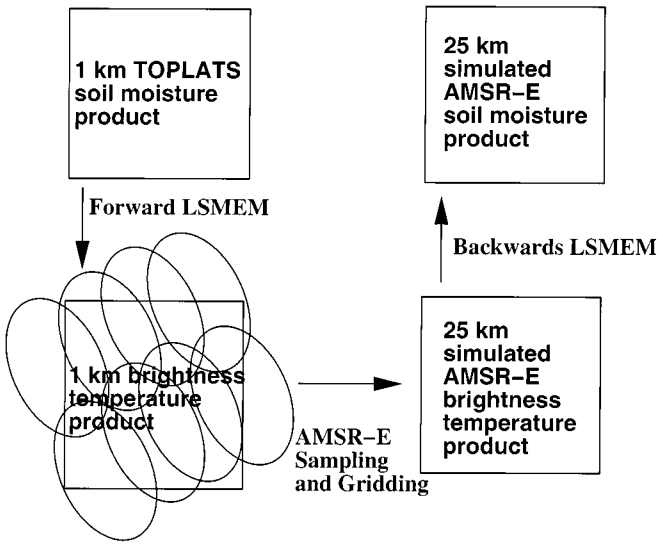

Fig. 1. Schematic diagram of the OSSE procedure.

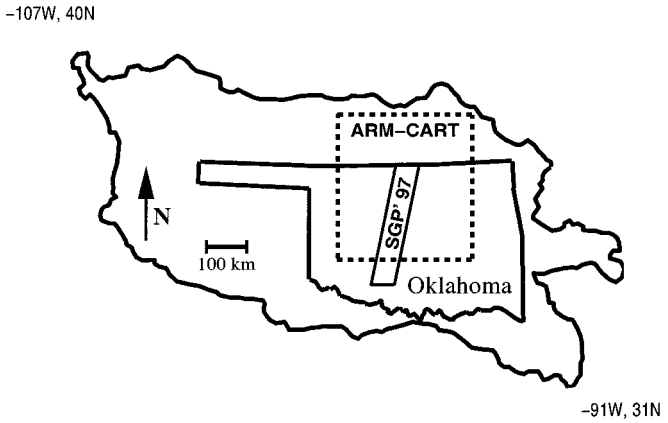

Fig. 2. Location of Red-Arkansas River basin within the U.S. Southern Great Plains. Also shown are the ARM-CART site boundaries and SGP'97 transect.

retrieval and processing of AMSR-E products are represented using angled bracket $\langle\rangle$ notation. To reflect current processing plans, T_b retrievals were gridded into 25-km grid-cells. The gridded T_b product retrieved by the AMSR-E sensor can be represented as

$$\langle f(\theta, T_s, \tilde{x})\rangle = \langle T_b\rangle. \tag{2}$$

The LSMEM represented in (1) can be inverted to convert inputs of T_b into θ

$$f^{-1}(T_b, T_s, \tilde{x}) = \theta. \tag{3}$$

This backward LSMEM process was applied to the gridded T_b imagery produced using (2). Since the backward process was run at the 25-km grid-scale, the land surface parameters represented by $\tilde{x}$ in (1), as well as T_s were linearly averaged up to 25 km. Square brackets [ ] are used to represent taking a simple linear average. Using this notation, the grid-scale AMSR-E soil moisture product can be represented as $f^{-1}(\langle T_b\rangle, [T_s], [\tilde{x}])$.

TABLE I
NOTATION FOR VARIOUS 25-km SOIL MOISTURE PRODUCTS

Notation	Description of Soil Moisture Product
$[\theta]$	Linearly averaged soil moisture
$\{\theta\}_c$	Center 1 km pixel sampled within each 25 km pixel
$\{\theta\}_n$	Mean of n 1 km pixels sampled within each 25 km pixel
$f^{-1}(\langle T_b \rangle)$	Inversion based on AMSR-E retrieved and gridded T_b
$f^{-1}([T_b])$	Inversion based on linearly averaged T_b

The critical issue is the degree to which this simulated AMSR-E soil moisture product differs from a linear aggregation of the original 1-km soil moisture imagery at (or above) the -3 dB resolution of the AMSR-E antenna ($\sim 60^2$ km^2). As discussed earlier, differences between the products are attributable to a combination of inconsistencies in spatial support due to gain function sampling effects and nonlinearities in the backward LSMEM process. Replacing $\langle T_b \rangle$ with a simple linear average $[T_b]$ eliminates error in the imagery due to gain function sampling effects, however, unless the backward LSMEM process f^{-1} is linear with respect to all inputs

$$f^{-1}([T_b],[T_s],[\tilde{x}]) \neq [\theta]. \tag{4}$$

Comparison of $[\theta]$ and $f^{-1}([T_b],[T_s],[\tilde{x}])$ highlights the effects of nonlinearities in the microwave retrieval of soil moisture. While comparison of $[\theta]$ and $f^{-1}(\langle T_b \rangle,[T_s],[\tilde{x}])$ reflects the impact of both nonlinearities in the LSMEM and antenna gain function sampling effects.

Two additional products, $\{\theta\}_c$ and $\{\theta\}_n$, were also constructed to examine the performance of various validation strategies. The first strategy ($\{\theta\}_c$) was based on sampling the 1-km soil moisture pixel at the center of each 25-km grid-cell in the original hydrologic model output and using this sampled value to characterize the entire $25^2 -$ km^2 grid-cell area. The second set of products ($\{\theta\}_n$) was based on spatial averages obtained through a random sample of n 1-km soil moisture pixels within each 25-km grid-cell. The validation strategies provide an opportunity to assess the degree to which differences between the benchmark imagery $[\theta]$, and imagery derived from microwave remote sensing $f^{-1}(\langle T_b \rangle,[T_s],[\tilde{x}])$ can be quantified based on information sampled at the 1-km field-scale.

Analysis will focus on comparing the benchmark soil moisture imagery $[\theta]$ to the simulated AMSR-E soil moisture products $f^{-1}(\langle T_b \rangle,[T_s],[\tilde{x}])$ and $f^{-1}([T_b],[T_s],[\tilde{x}])$ and the simulated validation soil moisture products $\{\theta\}_c$ and $\{\theta\}_n$. Comparisons will be made at a range of scales up to and beyond the ~ -3 dB resolution of the sensor. For convenience, $f^{-1}(\langle T_b \rangle,[T_s],[\tilde{x}])$ will be referred to as $f^{-1}(\langle T_b \rangle)$ and $f^{-1}([T_b],[T_s],[\tilde{x}])$ as $f^{-1}([T_b])$. Notation for 25-km soil moisture products is summarized in Table I. All soil moisture values will be given in terms of volumetric percentages ($100 * \text{cm}^3_{\text{water}}/\text{cm}^3_{\text{soil}}$). The following sections will describe each component of the OSSE procedure in greater detail.

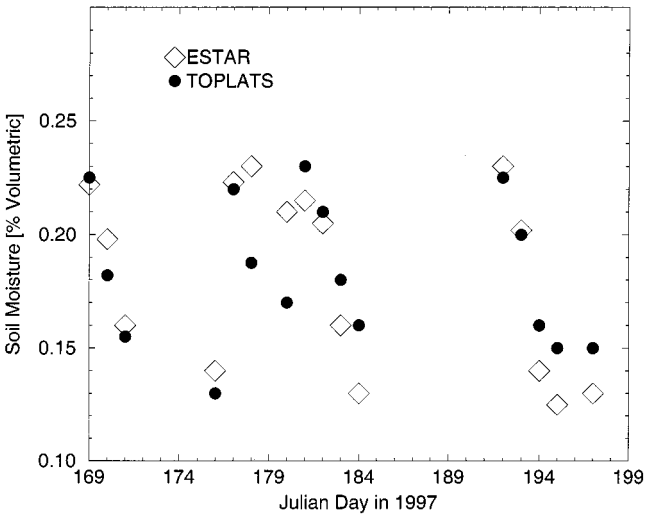

Fig. 3. Modeled (TOPLATS) versus remotely sensed (ESTAR) surface soil moisture results for the entire SGP'97 transect during the SGP'97 field campaign.

A. TOPLATS Hydrologic Modeling

Noon surface (5 cm) soil moisture and surface temperature data were obtained by running the hydrological model TOPLATS (TOPMODEL-based land-surface-atmosphere transfer scheme) [16] on a 1-km grid over the entire 575 000 km^2 Red-Arkansas River basin in the south-central United States (Fig. 2) from April 1, 1994 to July 31, 1994. TOPLATS calculates a full water balance for three soil layers and incorporates TOPMODEL concepts to describe the lateral redistribution of subsurface water in response to topographic and soil texture variability [17], [18]. Using soil moisture information provided by the water balance, the model derives a surface temperature by numerically solving the surface energy balance equation. Model input was derived from a number of high resolution data sets including 4-km WSR-88D precipitation imagery, 1 km GOES solar radiation imagery, spatially interpolated NCDC surface airways meteorology data, and 1-km soil and vegetation classifications. The model was calibrated using naturalized stream flow data for five subcatchments of the Red-Arkansas River basin. Initial conditions were calculated by running a low-resolution version of TOPLATS over 314 subcatchments of the Red-Arkansas basin from April 1, 1992 to April 1, 1994.

Both the water and the energy balance component of TOPLATS have been extensively validated at the point-scale for sites within the U.S. Southern Great Plains [16], [19]. More recent work has focused on validation at larger spatial scales. Fig. 3 shows comparisons made during the 1997 Southern Great Plains (SGP'97) field experiment between TOPLATS modeled surface soil moisture and estimated soil moisture based on ESTAR (L-band) microwave remote sensing over the SGP'97 transect shown in Fig. 2 [20]. No large-scale soil moisture data sets were available for the time period studied here (1994 growing season), but the energy balance portion of the model performs very well when compared to spatially averaged flux tower data within the $360^2 -$ km^2 ARM-CART study site (Figs. 2 and 4).

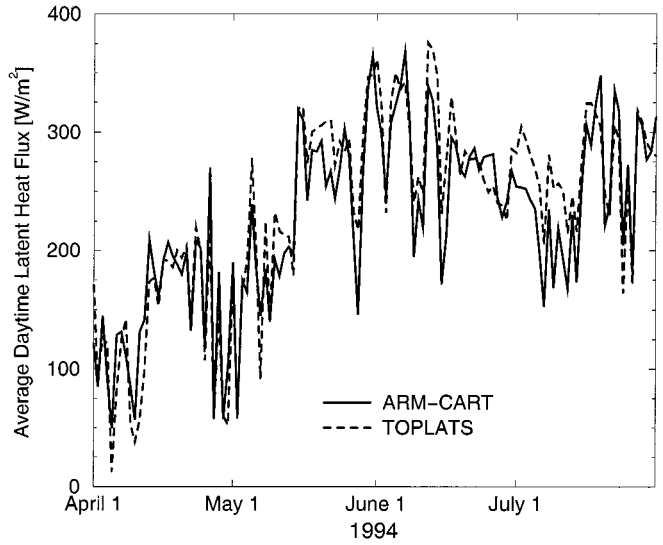

Fig. 4. Modeled (TOPLATS) versus *in situ* measured (ARM-CART bowen ratio towers) daily averages of latent heat flux for the entire ARM-CART domain during the 1994 growing season.

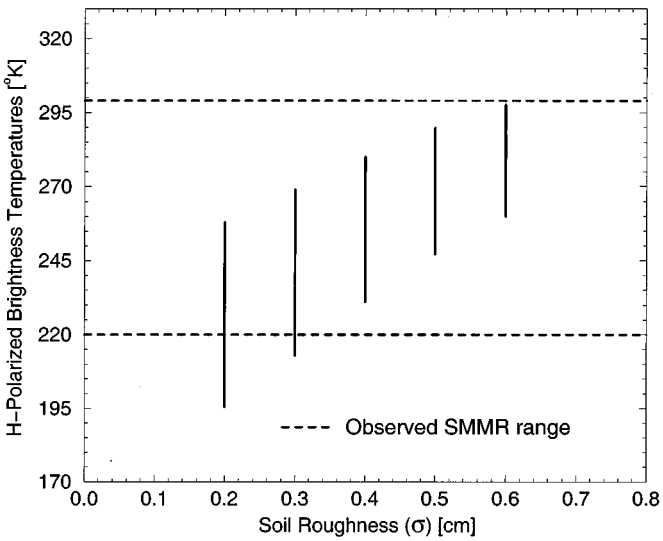

Fig. 5. Dynamic range of simulated horizontally-polarized brightness temperature data at a spatial resolution of 1.5° between May 1, 1994 and July 31, 1994 versus soil roughness (σ). Also shown is the dynamic range observed for similar measurements made by the scanning multichannel microwave radiometer (SMMR) at 6.6 GHz [33].

B. Land Surface Microwave Emission Modeling

The land surface microwave emission model (LSMEM) as described in [21] was implemented to simulate brightness temperatures at the top of a canopy layer. All simulations were based on noontime soil moisture and surface temperature results derived from TOPLATS modeling. The dielectric constant of the soil was computed after [22], and the dielectric constant of water was parameterized after [23]. The reflectivity of the smooth surface can either be calculated using the plane stratified media model proposed by [24] or the two layer model published in [25] and [26]. Since TOPLATS calculations provide integrated water contents for the top 5-cm soil layer, the two layer model was used in this study, and the rough soil emissivity was then calculated after [27]. The vegetation was taken into account following [28]. The atmospheric contributions to the TOA brightness temperature at 6.9 GHz were found to be small [29]. Moreover, water vapor and cloud liquid water produce only little variation at this specific frequency [29]. Therefore, no atmospheric effects were considered in this study.

The single scattering albedo and the vegetative structure coefficient were held constant at 0.04 [30] and 0.0027 [21], respectively, for all vegetation and soil texture types. Clay and sand percentages and soil bulk density values were assigned according to the STATSGO soil texture classification and the USDA soil triangle. One soil layer with a depth of 5 cm was assumed. This is likely deeper than the true penetration depth of microwave measurements made at 6.9 GHz [31]. However, computational limitations demanded that some vertical resolution be sacrificed in order obtain the required horizontal detail.

Vegetative water content (VWC) values for agricultural crops were chosen to match those measured during the SGP'97 experiment [6]. Values for grass and shrub areas were derived using the normalized difference vegetation index (NDVI)/VWC relationship presented by [6]

$$\mathrm{VWC}\left[\frac{\mathrm{kg}}{\mathrm{m}^2}\right] = 1.9134 * \mathrm{NDVI}^2 - .3214 * \mathrm{NDVI}. \qquad (5)$$

Because of a temporal gap in the data archive of advanced very high resolution radiometer (AVHRR) imagery during the 1994 growing season, NDVI values for the region were derived from imagery acquired during June 1995. The effective surface temperature T_s was derived from TOPLATS predictions of surface and deep soil temperature using the approximation presented by [32]. For vegetation fractional coverage, baseline values of 90% for forests, 80% for tall grass/crops, and 60% for short grass/shrubs areas were chosen and a sensitivity analysis, described in Section III-A, was performed to assess the impact of uncertainty in these values on results. The vegetation classification used did not distinguish between winter wheat and other agricultural crops. To compensate, 60% of the agricultural fields were assumed to be winter wheat and therefore contained no vegetation after a harvest date of June 1.

Surface soil roughness (RMS height σ [27]) values used in the OSSE were derived from comparisons of LSMEM results to spaceborne brightness temperature observations. Unfortunately, no validation data set for brightness temperatures near 6.9 GHz exists for the Southern Great Plains region during the 1994 growing season. As an alternative, LSMEM T_b results were compared to scanning multichannel microwave radiometer (SMMR) 6.6 GHz data from 1978 to 1987 processed at a 1.5° resolution [33]. The study area included sparsely vegetated areas in Texas as well as forested areas in Missouri. Results for the summer months (May to August) over the sparsely vegetated area give a day-time dynamic range in horizontally polarized brightness temperature of 218 to 299 K (Fig. 3 in [33]). For the heavily vegetated area, a dynamic range of 238 to 285 K was observed. Fig. 5 compares the dynamic range of 1.5°-scale brightness temperatures calculated between May and July 1994 using TOPLATS and the LSMEM for a range of σ values to the dynamic range observed in 8.5 years of pooled daytime growing-season (May to August) SMMR observations. A σ value of 0.4 cm was found to provide the best match to the

observed dynamic range. The slightly larger range observed in the SMMR data is probably due to a longer sampling period (8.5 years versus 1 year) as well as the inclusion of August in the SMMR data. Soil roughness measurements at small scales have resulted in values up to 0.36 cm for a spectral region from 4.5 to 7.4 GHz [34], [35]. However, if the parameterization of rough soil is simple and does not take into account the horizontal autocorrelation length the effective soil roughness at a 30° viewing angle was found to be larger (up to 0.8 cm) [34]. The functional dependency of the effective σ on viewing angle and frequency is almost unknown. Given that the calibrated value of 0.4 cm falls within the theoretical range given by [34], it was taken to be a representative σ value for the entire Red-Arkansas basin.

C. Simulation of AMSR-E Orbital and Sampling Characteristics

Based on the sun-synchronous orbit of the EOS-AQUA platform and scanning characteristics of the AMSR-E 6.925 GHz radiometer, hypothetical AMSR-E overpasses were simulated for a 60-day period starting June 1, 1994 using code provided by Dr. E. Njoku of NASA's Jet Propulsion Laboratory, Pasadena, CA. The orbital characteristics of the EOS-AQUA platform and the scan pattern of the AMSR-E sensor produced 153 overpasses with at least partial coverage of the Red-Arkansas River basin during that time period. For each overpass, a new scan pattern was mapped for every 10 km traveled by the sensor. The simulation simplified actual sensor behavior slightly by not incrementing satellite motion during the computation of each scan pattern. Within each scan, the simulation mapped the location of individual footprint locations to the surface of the earth. A full AMSR-E radiometer scan will contain 196 separate footprints locations. To ease the computational burden of the simulation, the location of only every tenth footprint along each scan was recorded. The remaining footprint centers were located using linear interpolation. Each footprint center was then used to take a weighted average of the simulated 1-km T_b field weighting given by the Gauss function approximation to the 6.925 GHz AMSR-E antenna gain function [4]. Scan patterns and antenna gain function sampling geometry for a single overpass of the Red-Arkansas River basin are shown in Fig. 6. Any footprint location where more than 10% of the gain function weighting fell outside of the TOPLATS domain was omitted from the analysis. Since the sampling rate of the sensor (one sample per 10^2 km^2) is smaller than the area of each grid-cell (25^2 km^2), multiple footprint centers will fall within a single 25-km grid-cell. All T_b retrievals whose footprint center fell within a given grid-cell were averaged (with equal weighting) to obtain a T_b value for the grid-cell. Any 25-km grid-cell that contained a footprint location omitted due to model domain edge effects was itself removed from the analysis.

D. Inversion of the LSMEM

An iterative root finder was used to numerically invert the LSMEM and convert gridded T_b fields back into soil moisture. Two separate fields were constructed in this way: soil moisture based on sampling of AMSR-E retrieval of T_b (i.e., $f^{-1}(\langle T_b \rangle, [T_s], [\tilde{x}])$) and soil moisture based on linear aggregation of T_b (i.e., $f^{-1}([T_b])$). In both cases, fields of 1-km T_s, soil clay and sand fractions, vegetation water content (VWC), and fractional vegetation cover were linearly averaged up to 25 km. Since VWC is strongly nonlinear with respect to T_b, linear aggregation will not necessarily produce the correct effective parameter value at 25 km. The use of a more sophisticated effective VWC parameter may reduce the magnitude of errors attributed to nonlinearities in the LSMEM. However, in this analysis such an effect is simply considered a contributor to error caused by the interaction of land surface heterogeneity with nonlinearities within the LSMEM.

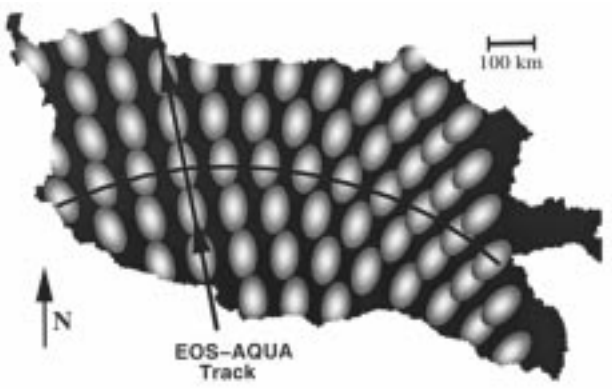

Fig. 6. Scan and -3 dB gain function patterns for a single AMSR-E overpass superimposed on the Red-Arkansas River basin. For display purposes, only every tenth gain function pattern in both the track and scan direction is shown.

For certain pixels, the impact of land surface heterogeneity is strong enough that gridded T_b values could not be inverted into a physically realistic soil moisture solution. In these cases, two separate strategies were employed. In the first, soil moisture values for these grid cells were set equal to a regionally averaged soil moisture value based on areas of the basin where T_b values were successfully inverted into soil moisture. The second strategy assigned soil moisture values to be either residual (for unrealisticly low results) or saturation moisture levels (for unrealisticly high results).

III. Results

Fig. 7 compares imagery of: the benchmark 25-km grid-scale soil moisture product $[\theta]$ derived from linear aggregation of the original 1-km TOPLATS field, the simulated *in situ* sampled field $\{\theta\}_c$ derived from sampling the center 1-km pixel found in each 25-km grid-cell, and the simulated AMSR-E soil moisture product $f^{-1}(\langle T_b \rangle)$ for a single day (June 30, 1994) during the 60-day simulation. Fig. 8 shows a 60-day time series of $[\theta]$, $\{\theta\}_c$ and $f^{-1}(\langle T_b \rangle)$ values for a typical 25-km grid-cell. Differences clearly exist between the three products.

A. Vegetation Effects

Large differences between $f^{-1}(\langle T_b \rangle)$ and $[\theta]$ occur primarily in the heavily vegetated eastern and extreme western edges of the Red-Arkansas River basin. The interplay between vegetation amount and sensitivity to land surface heterogeneity is not surprising due to the well known reduction in the sensitivity of T_b to soil moisture over heavily vegetated regions [36] and

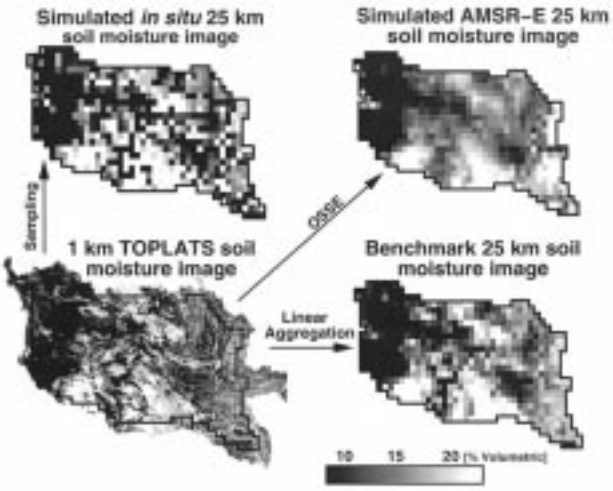

Fig. 7. Sample soil moisture imagery from a single day (June 30, 1994) of the simulation. Shown are examples of the simulated *in situ* $\{\theta\}_c$, simulated AMSR-E $f^{-1}(\langle T_b \rangle)$, and benchmark $[\theta]$ products. Also shown is the original TOPLATS 1-km soil moisture image from which all three products were derived.

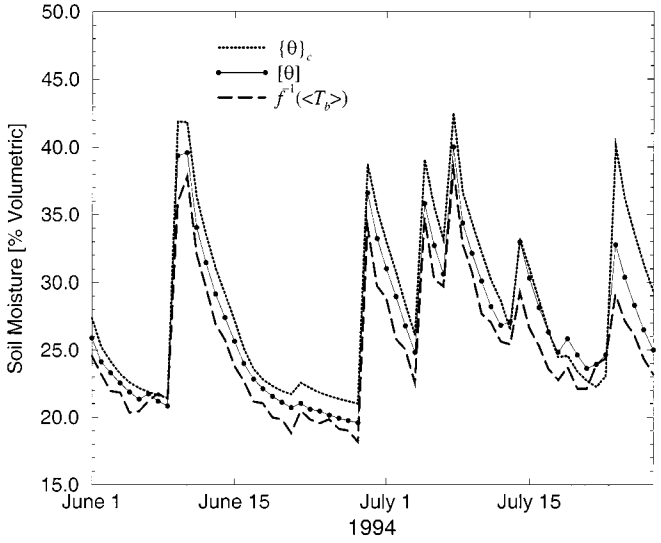

Fig. 8. Sample time series for a typical 25-km pixel within the Red-Arkansas River basin. Shown are examples of the simulated *in situ* $\{\theta\}_c$, simulated AMSR-E $f^{-1}(\langle T_b \rangle)$, and benchmark $[\theta]$ products.

the strong nonlinear relationship between VWC and T_b in the LSMEM. Fig. 9 plots the 50-km root-mean-squared (RMS) retrieval error ($f^{-1}(\langle T_b \rangle)$ versus $[\theta]$) associated with masking portions of the Red-Arkansas River basin that contain vegetative water content (VWC) values above a certain threshold. Results are taken from all imagery simulated between June 1 and July 31, 1994 and include both strategies for assigning soil moisture values to grid-cells with physically unrealistic retrievals (see Section II.D). Also plotted is the fraction of the basin—excluding areas masked due to edge effects—passing the VWC threshold criteria. The figure suggests that removing a handful of heavily vegetated pixels from the analysis significantly reduces retrieval error. For instance, in the case of assigning failed retrievals to the basin soil moisture mean, setting the VWC threshold to be 0.75 kg/m^2 masks only 10%

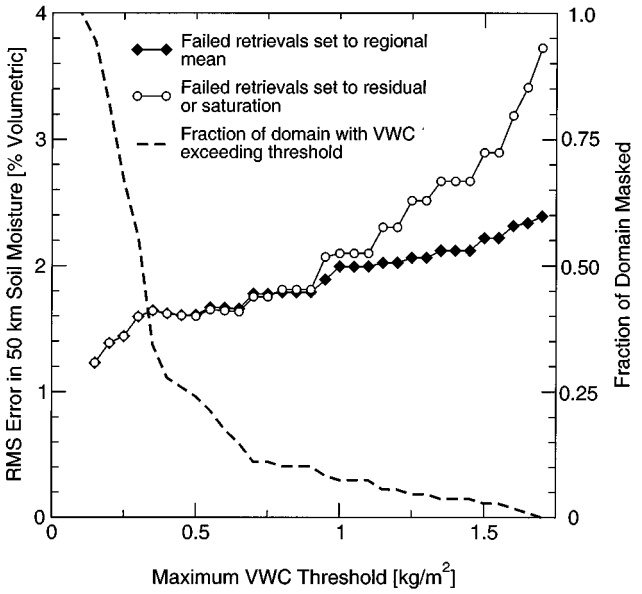

Fig. 9. Retrieval error ($f^{-1}(\langle T_b \rangle)$ versus $[\theta]$) at 50-km associated with masking portions of the Red-Arkansas River basin with VWC levels above a certain threshold. Also plotted are areal fractions of the basin that exceed the VWC threshold.

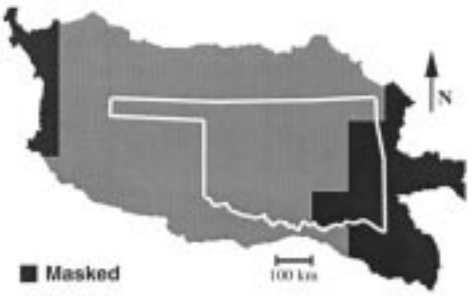

Fig. 10. Portion of the basin (in black) masked due to 100-km VWC values exceeding the 0.75 kg/m^2 threshold.

of the basin yet reduces absolute RMS retrieval errors from 2.4% (0.024 $\text{cm}^3_{\text{water}}/\text{cm}^3_{\text{soil}}$) to 1.8% volumetric. The impacts of lowering the VWC threshold are even more dramatic for the case of setting failed retrievals to residual or saturation. To ensure that reported errors are not inflated by the inclusion of heavily vegetated regions, surfaces with VWC values exceeding 0.75 kg/m^2 are masked from all subsequent calculations. Such masking also eliminates the sensitivity seen in Fig. 9 to the strategy selected for assigning values to grid-cells where soil moisture retrieval fails. Fig. 10 shows the portion of the basin exceeding a 100 km 0.75 kg/m^2 VWC threshold and provides a sense of the spatial domain over which subsequent results can be considered representative. The areal fraction masked in Fig. 10 appears larger than the fractions plotted in Fig. 9 since many of the heavily vegetation regions were already masked in the analysis based on their proximity to the basin boundary (see Section II-C).

The strong interplay between vegetation density and sensitivity to surface heterogeneity also suggests that results will be sensitive to the manner in which vegetation is parameterized. This is potentially problematic given the uncertainty surrounding reasonable fractional cover values for various vege-

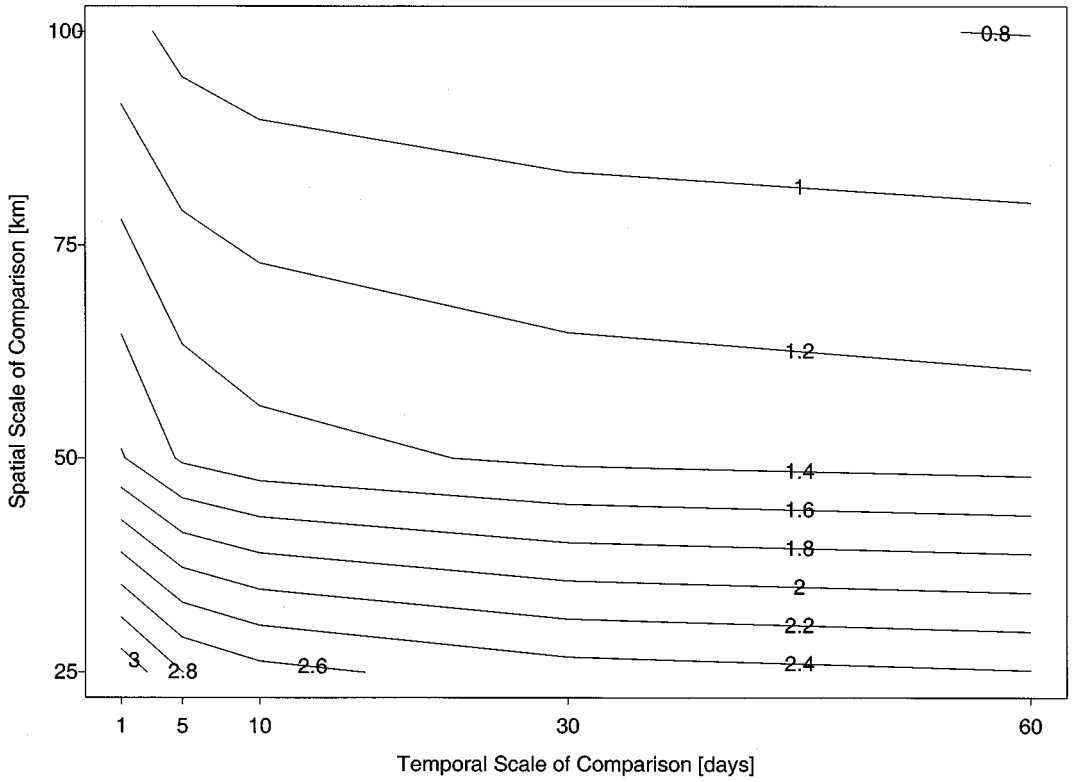

Fig. 11. Contour plot of average RMSE in percentage volumetric soil moisture for simulated AMSR-E products $f^{-1}(\langle T_b \rangle)$ at various spatial and temporal scales of comparison.

tation types. Originally, all vegetation classifications were assigned to one of three broad categories: forest, tall grass/crop, and short grass/shrubland. These three vegetation types were assigned default fractional vegetation covers of 90%, 80%, and 60%, respectively. Simulations were also performed for two other vegetation regimes during June 1994: a heavier regime that increased the fractional coverage of each classification by 10% and a lighter regime with coverage percentages decreased by 10%. The percentage changes were absolute, not relative. At the 50-km scale, moving from the light to heavy regime was associated with an increase in absolute RMS retrieval errors from 1.7% to 2.0% volumetric. Such low sensitivity over a wide range of fractional coverage values suggests that uncertainty concerning the true fractional vegetation coverage for the region will induce relative errors of less than 20% into results.

B. Time and Space Structure of Retrieval Errors

Differences between $[\theta]$ and $f^{-1}(\langle T_b \rangle)$ at various levels of aggregation in time and space are summarized in Fig. 11. At the finest time and space resolutions (1 day and 25 km), absolute RMSEs in the simulated AMSR-E products are on the order of 3.1% volumetric (0.031 $\mathrm{cm}^3_{\mathrm{water}}/\mathrm{cm}^3_{\mathrm{soil}}$). These errors fall as comparisons are made at coarser spatial scales. Absolute error levels of 1.8% and 1.1% volumetric soil moisture are found at 50 and 100 km respectively. The effects of temporal aggregation appear more muted. Summing $f^{-1}(\langle T_b \rangle)$ imagery up to 60 days results in only a 20% relative reduction in error levels, suggesting that retrieval errors are dominated by biases that persist up to seasonal time scales. Due to nonlinearites in the soil moisture retrieval process, the simulated AMSR-E soil moisture imagery is, on average, slightly drier than the benchmark imagery with an overall absolute bias of -0.2% volumetric. A time series of daily RMSEs (not shown) demonstrates that while absolute errors in soil moisture retrieval fall slightly during dry-down events, relative errors are essentially constant over the course of the simulation.

Errors in the $f^{-1}(\langle T_b \rangle)$ imagery are due to a combination of gain function sampling effects and the presence of nonlinearities in the backward LSMEM process. Comparing $f^{-1}([T_b])$ imagery, which utilizes a simple linear aggregation of T_b over each 25-km grid square, and $f^{-1}(\langle T_b \rangle)$ isolates the impact of gain function sampling effects. Likewise, differences between $f^{-1}([T_b])$ and benchmark results $([\theta])$ are due solely to nonlinearities in the LSMEM. Fig. 12 plots both comparisons. Between 25 and 100 km errors associated with antenna gain function sampling effects are clearly larger than those caused by nonlinearities in the LSMEM.

C. Time and Space Structure of Validation Error

The time and space structure of differences between the simulated AMSR-E retrievals $(f^{-1}(\langle T_b \rangle))$ and the simulated imagery derived from *in situ* sampling $(\{\theta\}_c)$ are shown in Fig. 13. These results simulate the ability of a field-scale sampling strategy on a fixed 25-km grid to validate AMSR-E results. On a daily time scale, absolute RMS differences of 7.2%, 3.3%, and 1.8% were found at 25, 50, and 100 km respectively. As in Fig. 11, temporal aggregation in Fig. 13 has little effect on the observed RMSEs. The differences seen in Fig. 13

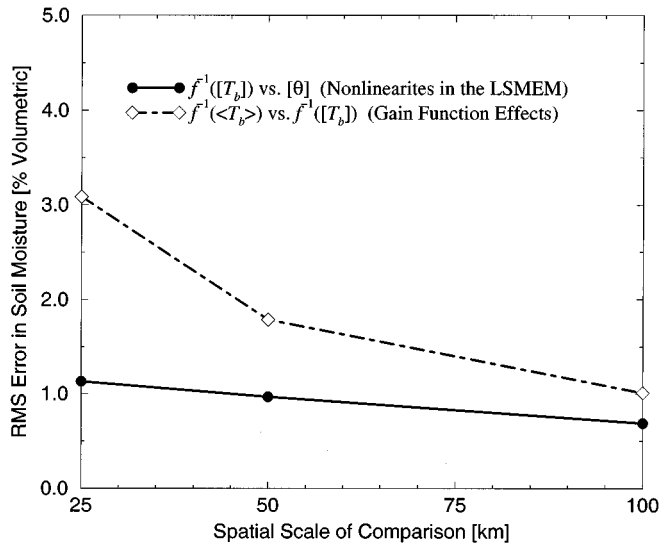

Fig. 12. Decomposition of total retrieval error into components due to nonlinearities in the LSMEM ($f^{-1}([T_b])$ versus $[\theta]$) and antenna gain function sampling effects ($f^{-1}(\langle T_b \rangle)$ versus $f^{-1}([T_b])$).

are comprised of both AMSR-E retrieval errors ($f^{-1}(\langle T_b \rangle)$ versus $[\theta]$) and the validation errors associated with attempting to characterize a 25-km grid-cell with a single 1-km sample. At a daily time step, Fig. 14 plots the observed differences between retrieval and validation products for a range of *in situ* sampling strategies. As the density of soil moisture sampling increases, the total observational error ($f^{-1}(\langle T_b \rangle)$ versus $\{\theta\}_n$ or $\{\theta\}_c$) converges onto the retrieval error ($f^{-1}(\langle T_b \rangle)$ versus $[\theta]$).

IV. Discussion and Conclusions

This observation system simulation experience (OSSE) deals solely with the impact of land surface heterogeneity on the accuracy of soil moisture products derived from passive microwave remote sensing. Other potential sources of error in satellite remote sensing products are ignored. For instance, the same microwave emission model and parameters are used in the forward LSMEM as are used in the backward retrieval of soil moisture. The quality of the model calibration is degraded only by scale effects and nonlinearities associated with averaging parameters and reapplying the model at a coarser grid-scale (25 km). In reality, ignorance of the true radiative transfer parameterization will constitute a major source of error in microwave soil moisture retrieval at 6.9 GHz, especially over vegetated surfaces [36]. In addition, spatial heterogeneity in both soil roughness (σ) and the vegetation structure coefficient was not represented in this analysis. More detailed representations of these land surface parameters would likely enhance nonlinear effects and increase retrieval errors.

Sensitivity to spatial heterogeneity is positively correlated with the density of vegetation cover. Fig. 9 demonstrates that retrieval errors are sensitive to the choice of a threshold for masking densely vegetated regions and that a large portion of the errors found within the Red-Arkansas basin are concentrated in a relatively small number of heavily vegetated grid cells. A VWC threshold of 0.75 kg/m^2 was chosen as a tradeoff between minimizing the impact of densely vegetated and maximizing the analysis domain area. This threshold is half of the ~ 1.5 kg/m^2 value given as a threshold for AMSR-E soil moisture retrieval [5]. The inclusion of areas up to the 1.5 kg/m^2 level increases retrieval errors by about 20% if nonretrievable pixels are set to a basin mean and 100% if physically unrealistic retrievals are set to either saturation or residual (Fig. 9). Clearly, the first strategy is preferable if surfaces with VWC values above 0.75 kg/m^2 are to be included in operational soil moisture retrievals.

Despite the potential underestimation of heterogeneity and relatively conservative masking of vegetation, results suggest that land surface heterogeneity will impact the quality of AMSR-E soil moisture products. The stated accuracy goal for AMSR-E soil moisture retrieval is 0.06 g/cm^3 ($\sim$ 6% volumetric soil moisture or 0.06 $\text{cm}^3_{\text{water}}/\text{cm}^3_{\text{soil}}$) at scales equivalent to the -3 dB resolution of the AMSR-E antenna ($\sim 60^2$ km^2) [5]. Fig. 11 suggests that, for daily imagery, scale effects alone will produce absolute errors of 1.7% volumetric (0.017 $\text{cm}^3_{\text{water}}/\text{cm}^3_{\text{soil}}$) when comparisons are made at 60 km. This error is comprised of two separate components: error associated with obtaining gridded products from sampling heterogeneous T_b fields with nonlinear gain functions and effects associated with the interaction of nonlinearities in LSMEM processes with land surface heterogeneity. Fig. 12 demonstrates that the gain function sampling error is greater than the effect of nonlinearities in LSMEM processes. The conclusion that the impact of LSMEM nonlinearities is relatively minor compared to other potential error sources is consistent with results from previous studies [13], [15].

Fig. 13 summarizes the simulated differences between field-scale *in situ* samples and AMSR-E soil moisture products. At the -3 dB resolution-scale of the AMSR-E antenna (~ 60 km), the observed RMS difference between *in situ* measurements, sampled on a fixed 25-km grid, and simulated AMSR-E products is 3.0% (0.03 $\text{cm}^3_{\text{water}}/\text{cm}^3_{\text{soil}}$). Validation errors can be reduced through denser sampling grids and/or the application of more sophisticated spatial statistics (i.e., interpolation or block kriging). However, it should be noted that the 1-km field-scale support of the simulated validation measurements compares favorably to the essentially point-scale samples taken within operational soil moisture networks. In addition, the 25-km sample spacing used is finer than the spacing found within the Illinois Water Survey Network (93 km), the Oklahoma Mesonet Network (35 km), or the Southern Great Plains ARM-CART network (> 50 km) [11]. Fig. 14 demonstrates the advantage of denser sampling strategies that may be feasible within specialized soil moisture validation networks or during intensive field campaigns.

One hope has been that validation and retrieval errors associated with spatial heterogeneity can be filtered through aggregation in time. Figs. 10 and 13 suggest that up to time scales of 60 days, such a strategy will not appreciably reduce offsets between AMSR-E soil moisture products and either benchmark products (Fig. 10) or *in situ* field-scale measurements (Fig. 13). Fig. 8 shows a two-month time series of $[\theta]$, $\{\theta\}_c$, and $f^{-1}(\langle T_b \rangle)$ values for a typical 25-km grid-cell. Despite sampling a number of consecutive rainfall/dry-down cycles and a range of hydrologic conditions, both the validation error ($\{\theta\}_c - [\theta]$) and the AMSR-E retrieval error ($f^{-1}(\langle T_b \rangle) - [\theta]$)

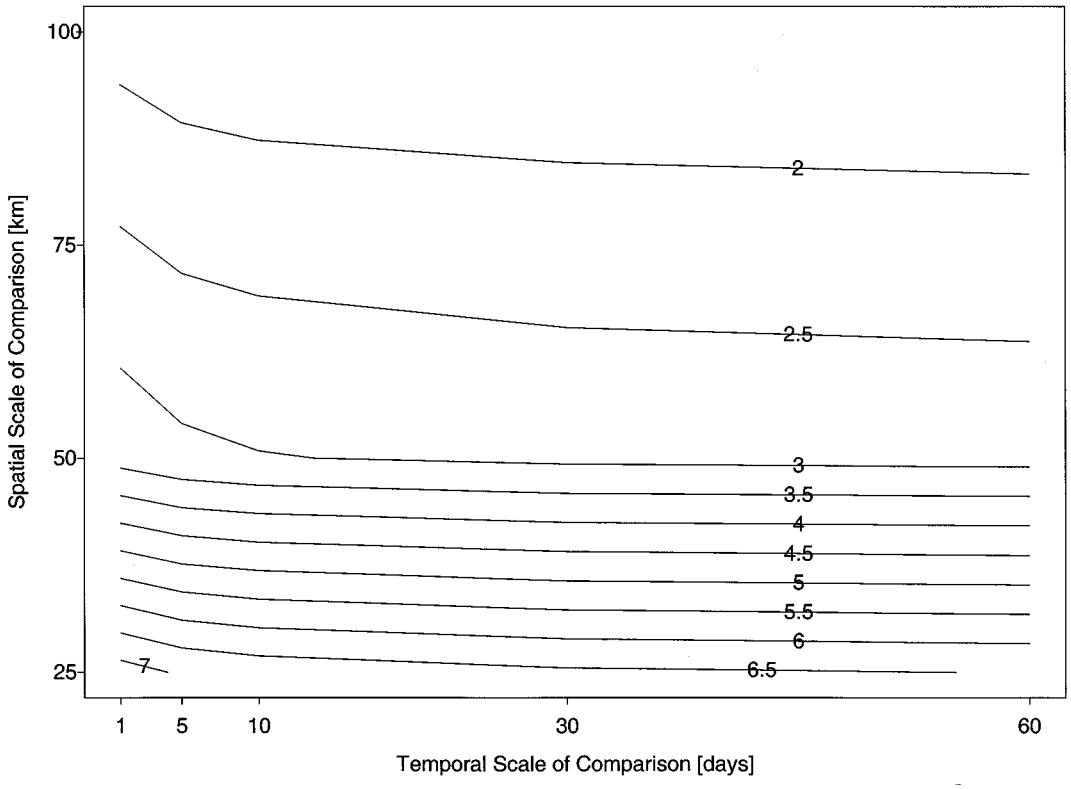

Fig. 13. Contour plot of average RMS difference in percentage volumetric soil moisture between the simulated validation $\{\theta\}_c$ and AMSR-E $f^{-1}(\langle T_b \rangle)$ products at various spatial and temporal scales of comparison.

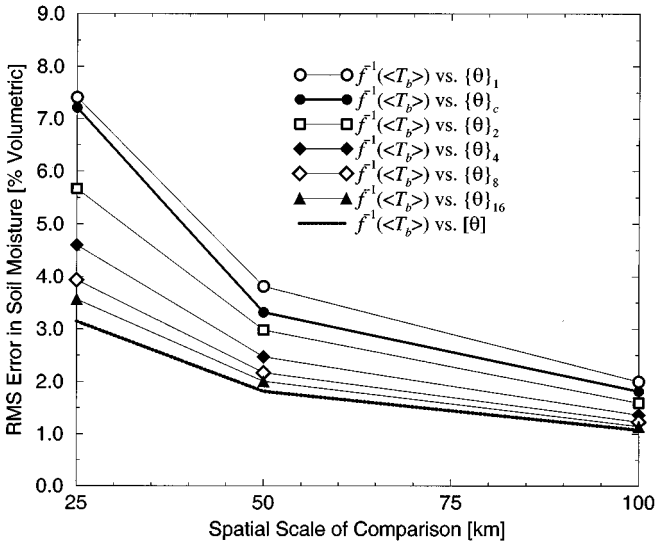

Fig. 14. RMS differences between simulated AMSR-E products $f^{-1}(\langle T_b \rangle)$ and the validation validation products $\{\theta\}_c$ (a single 1-km sample at the center of each 25-km pixel) and $\{\theta\}_n$ (n random 1-km samples taken within each 25-km pixel) for a range of n. For large n, the differences converge to those associated with AMSR-E retrieval error ($f^{-1}(\langle T_b \rangle)$ versus $[\theta]$).

generally retain the same sign throughout the entire period. These results suggest that TOPLATS and the LSMEM attribute a substantial portion of the land surface heterogeneity responsible for these errors to heterogeneity in vegetation, soil, and topographic forcings that vary only at seasonal time scales and above. Sampling across the randomizing effects of AMSR-E gain function patterns (which vary slightly from overpass to overpass) and dry-down/wet-up dynamics with daily to weekly time scales is not an effective way of filtering validation and retrieval errors associated with land surface heterogeneity.

While hampering filtering attempts, the persistence of a relatively constant bias in simulated AMSR-E retrievals suggests that spatial heterogeneity will not prevent validation and retrieval products from accurately representing temporal fluctuations in coarse-scale soil moisture. Such a simplistic temporal error structure may lend itself to correction through either calibration adjustments in the retrieval process or assimilation techniques that combine model predictions of surface soil moisture with AMSR-E retrievals.

ACKNOWLEDGMENT

The authors would like to thank Dr. E. Njoku of the NASA Jet Propulsion Laboratory, Pasadena, CA, for providing the software to simulate the orbital and scanning characteristics of the AMSR-E sensor. The NDVI image used was obtained from the EROS data center DAAC.

REFERENCES

[1] J. D. Michaud and W. J. Shuttleworth, "Executive summary of the Tucson Aggregation Workshop," *J. Hydrol.*, vol. 190, pp. 176–181, 1994.

[2] *Land Surface Processes in Atmospheric General Circulation Models*, P. S. Eagleson, Ed., Cambridge Univ. Press, New York, 1982.

[3] J. B. Stewart, E. T. Engman, R. A. Feddes, and Y. Kerr, Eds., *Scaling Up in Hydrology Using Remote Sensing*. New York: Wiley, 1996, p. 255.

[4] M. Drusch, E. F. Wood, and R. Lindau, "The impact of the SSM/I antenna gain function on land surface parameter retrieval," *Geophys. Res. Lett.*, vol. 26, pp. 3481–3484, Sept 1999.

[5] R. Spencer, F. Wentz, C. Kummerow, T. Wilheit, R. Ferraro, D. Cavalieri, J. Comiso, A. Chang, and E. Njoku, AMSR-E Science Data Validation Plan: Version 2, Available [Online]: http://eospso.gsfc.nasa.gov/validation/pmval.html.

[6] T. J. Jackson, D. M. Le Vine, A. Y. Hsu, A. Oldak, P. J. Starks, C. T. Swift, J. D. Isham, and M. Haken, "Soil moisture mapping at regional scales using microwave radiometry: The southern great plains hydrology experiment," *IEEE Trans. Geosci. Remote Sensing*, vol. 37, pp. 2136–2151, Sept. 1999.

[7] A. W. Western and G. Bloschl, "On the spatial scaling of soil moisture," *J. Hydrol.*, vol. 217, pp. 203–224, 1999.

[8] R. Lindau and E. Ruprecht, "SSM/I derived total water vapor content over the baltic sea compared to independent data," *Meterol. Zeitschr.*, vol. 9, pp. 117–123, Feb. 2000.

[9] M. A. Charpentier and P. M. Groffman, "Soil moisture variability within remote sensing footprints," *J. Geophys. Res.*, vol. 97, pp. 18 987–18 995, 1992.

[10] J. S. Famiglietti, J. A. Devereaux, C. A. Laymon, T. Tsegaye, P. R. Houser, T. J. Jackson, S. T. Graham, M. Rodell, and P. J. van Oevelen, "Ground-based investigation of soil moisture variability within remote sensing footprints during the southern great plains 1997 (SGP97) hydrology experiment," *Water Resources Res.*, vol. 35, pp. 1839–1851, 1999.

[11] Y. V. Vinnikov, A. Robuck, S. Qiu, and J. K. Entin, "Optimal design of surface networks for observation of soil moisture," *J. Geophys. Res.*, vol. 104, pp. 19 743–19 749, 1999.

[12] R. B. Grayson and A. W. Western, "Toward areal estimation of soil water content from point measurements: Time and space stability of mean response," *J. Hydrol.*, vol. 207, pp. 68–82, 1998.

[13] M. Drusch, E. F. Wood, and C. Simmer, "Up-scaling effects in passive microwave remote sensing: ESTAR 1.4 GHz measurements during SGP'97," *Geophys. Res. Lett.*, vol. 26, pp. 879–882, 1999.

[14] E. G. Njoku, S. J. Hook, and A. Chehbouni, "Effects of surface heterogeneity on thermal remote sensing of land parameters," in *Scaling up in Hydrology Using Remote Sensing*, J. B. Stewart, E. T. Engman, R. A. Feddes, and Y. Kerr, Eds. New York: Wiley, 1996, pp. 19–39.

[15] J. F. Galantowicz, D. Entekhabi, and E. G. Njoku, "Estimation of soil-type heterogeneity effects in the retrieval of soil moisture from radiobrightness," *IEEE Trans. Geosci. Remote Sensing*, vol. 38, pp. 312–316, Jan. 2000.

[16] C. D. Peters-Lidard, M. S. Zion, and E. F. Wood, "A soil-vegetation-atmosphere transfer scheme for modeling spatially variable water and energy balance processes," *J. Geophys. Res.*, vol. 102, pp. 4303–4324, 1997.

[17] K. J. Beven and M. J. Kirkby, "A physically based, variable contributing area model of basin hydrology," *Hydrol. Sci. Bull.*, vol. 24, no. 1, pp. 43–69, 1979.

[18] E. F. Wood, M. Sivipalan, K. Beven, and L. Band, "Effects of spatial variability and scale with implications to hydrologic modeling," *J. Hydrol.*, vol. 102, pp. 29–47, 1988.

[19] C. D. Peters-Lidard, "The effects of land surface heterogeneity on land–atmosphere interactions,", Ph.D. dissertation, Princeton Univ., Dept. Civil Environ. Eng., Princeton, NJ, 1997.

[20] C. Fernandez-Illescas and E. F. Wood, "Detailed water and energy balance modeling for the SGP'97 experiment," in *79th AMS Annu. Meeting*, Dallas, TX, Jan. 1999.

[21] Y. H. Kerr and E. G. Njoku, "A semiempirical model for interpreting microwave emission from semiarid land surfaces as seen from space," *IEEE Trans. Geosci. Remote Sensing*, vol. 28, pp. 384–393, May 1990.

[22] J. R. Wang and T. J. Schmugge, "An empirical model for the complex dielectric permittivity of soils as a function of water content," *IEEE Trans. Geosci. Remote Sensing*, vol. GE–18, pp. 288–295, Oct 1980.

[23] L. A. Klein and C. T. Swift, "An improved model for the dielectric constant of sea water at microwave frequencies," *IEEE Trans. Antennas Propagat.*, vol. AP–25, pp. 104–111, 1977.

[24] T. T. Wilheit, "Radiative transfer in a plane stratified dielectric," *IEEE Trans. Geosci. Remote Sensing*, vol. GE–16, pp. 138–143, Jan. 1978.

[25] L. Tsang, J. A. Kong, and R. T. Shin, *Theory of Microwave Remote Sensing*. New York: Wiley, 1985.

[26] F. W. Ulaby, R. K. Moore, and A. K. Fung, *Microwave Remote Sensing: Active and Passive*. Norwell, MA: Artech House, 1982, vol. III.

[27] B. J. Choudhury, T. J. Schmugge, A. Chang, and R. W. Newton, "Effect of surface roughness on the microwave emission from soils," *J. Geophys. Res.*, vol. 84, pp. 5699–5706, 1979.

[28] K. P. Kirdiashev, A. A. Chukhlantsev, and A. M. Shutko, "Microwave radiation of the earth's surface in the presence of vegetation," *Radio Eng. Electron.*, vol. 24, pp. 256–264, 1979.

[29] M. Drusch, E. F. Wood, and T. J. Jackson, "Vegetative and atmospheric corrections for soil moisture retrieval from passive microwave remote sensing data: Results from the southern great plains hydrology experiment 1997," *J. Hydrometeorol.*, vol. 2, pp. 181–192, 2001.

[30] Y. H. Kerr and J. P. Wigneron, "Vegetation models and observations—a review," in *Passive Microwave Remote Sensing of Land–Atmosphere Interactions*, B. J. Choudhury, Y. H. Kerr, E. G. Njoku, and P. Pamploni, Eds. Utrecht, The Netherlands, 1995, pp. 317–344.

[31] M. B. Owe and A. A. Van de Griend, "Comparison of soil moisture penetration depths for several bare soils at two microwave frequencies and implications for remote sensing," *Water Resources Res.*, vol. 34, pp. 2319–2327, 1998.

[32] B. J. Choudhury, T. J. Schmugge, and T. Mo, "A parameterization of effective temperature for microwave emission," *J. Geophys. Res.*, vol. 87, pp. 1301–1304, 1982.

[33] N. U. Ahmed, "Estimating soil moisture from 6.6 GHz dual polarization, and/or satellite derived vegetation index," *Int. J. Remote Sensing*, vol. 16, pp. 687–708, 1995.

[34] W. P. Waite, K. R. Cook, and B. B. Bryan, "A broad spectrum microwave system for remotely measuring soil moisture content," Tech. Rep., Center Univ. Arkansas, Fayetteville, 1973.

[35] G. D. Hancock, "Broad spectrum microwave measurement of rough discontinuous surfaces for the determination of moisture content," Dept. Elect. Eng., Univ. Arkansas, Little Rock, 1976.

[36] T. J. Jackson, "Measuring surface soil moisture using passive microwave remote sensing," *Hydrol. Process.*, vol. 7, pp. 139–152, 1993.

Wade T. Crow received the Ph.D. degree in civil and environmental engineering from Princeton University, Princeton, NJ, in 2001. His Ph.D. research focused on scale issues surrounding the microwave retrieval of soil moisture and the eventual assimilation of this imagery into weather prediction models.

He is currently a Postdoctoral Research Associate at Princeton University.

Dr. Crow received an Outstanding Student Paper Award at the 2000 Spring American Geophysical Union (AGU) Meeting for a portion of his dissertation.

Matthias Drusch received the Ph.D. degree from the Department of Meteorology, University of Bonn, Bonn, Germany, in 1998.

He is currently a Research Associate with the Bonn Meteorological Institute, Bonn. His research interests include application of microwave remote sensing to meteorology and hydrology and microwave emission modeling of the land surface.

Eric F. Wood received the Sc.D. degree from the Massachusetts Institute of Technology, Cambridge, in 1974.

He is currently a Professor with the Department of Civil and Environment Engineering, Princeton University, Princeton, NJ. His research interests include hydrological modeling at a variety of spatial scales, the application of remote sensing to hydrology, and the role of land surface processes in weather prediction models. He has been actively involved in developing the hydrologic application of Earth Observing System (EOS)-era remote sensors and was a SIR-C investigator carrying out research related to soil moisture estimation.

Dr. Wood is a Fellow of the American Geophysical Union (AGU) and a Fellow of the American Meteorological Society. He has received the AGU's Robert E. Horton Award and was the American Meteorological Society's 2001 Robert Horton Lecturer.